ADVANCES IN ATMOSPHERIC SCIENCES, VOL. 28, NO. 1, 2011, 178–186

Application of ATOVS Radiance-Bias Correction to Typhoon Track Prediction with Ensemble Kalman Filter Data Assimilation

CUI Limei[1,2] (崔丽梅), SUN Jianhua*[2] (孙建华), QI Linlin[3] (齐琳琳), and LEI Ting[2] (雷 霆)

[1] *College of Physical and Environmental Oceanography, Ocean University of China, Qingdao* 266100

[2] *Laboratory of Cloud-Precipitation Physics and Severe Storms, Institute of Atmospheric Physics, Chinese Academy of Sciences, Beijing* 100029

[3] *Institute of Aeronautical Meteorology and Chemical Defense, Equipment Academy of the Air Force, Beijing* 100085

(Received 10 February 2010; revised 20 April 2010)

ABSTRACT

In this paper, firstly, the bias between observed radiances from the Advanced TIROS-N Operational Vertical Sounder (ATOVS) and those simulated from a model first-guess are corrected. After bias correction, the observed minus calculated (O–B) radiances of most channels were reduced closer to zero, with peak values in each channel shifted towards zero, and the distribution of O–B closer to a Gaussian distribution than without bias correction. Secondly, ATOVS radiance data with and without bias correction are assimilated directly with an Ensemble Kalman Filter (EnKF) data assimilation system, which are then adopted as the initial fields in the forecast model T106L19 to simulate Typhoon Prapiroon (2006) during the period 2–4 August 2006. The prediction results show that the assimilation of ATOVS radiance data with bias correction has a significant and positive impact upon the prediction of the typhoon's track and intensity, although the results are not perfect.

Key words: ATOVS radiance, scan bias correction, air mass bias correction, Ensemble Kalman Filter (EnKF), Typhoon Prapiroon

Citation: Cui, L. M., J. H. Sun, L. L. Qi, and T. Lei, 2011: Application of ATOVS radiance-bias correction to typhoon track prediction with Ensemble Kalman Filter data assimilation. *Adv. Atmos. Sci.*, **28**(1), 178–186, doi: 10.1007/s00376-010-9145-9.

1. Introduction

China is a country seriously affected by tropical cyclones. Landing most frequently in the southeast, typhoons lead not only to damage caused by flooding, but also due to their severe winds and storm tides. In order to reduce the socioeconomic impacts, it is important to improve our ability to predict the intensity and tracks of tropical cyclones. However, there are still many problems associated with tropical cyclone forecasting in China, as well as in many developed countries (Chen, 1997; Chen and Meng, 2001). The difficulties include many factors, such as insufficient observations over the oceans, inaccurate parameterizations of the physical processes, and coarse model resolutions (Ding, 1991). The lack of sufficient observational data over the open sea in particular has been one of the major obstacles for studying the inner structure of tropical cyclones accurately (Meng et al., 2002). Fortunately, with the development of numerical models and progress in atmospheric remote sensing techniques, such a problem can be mitigated by non-conventional observations in sparse-area data, appropriate and advanced assimilation methods, and ensemble forecasting.

The emergence of the meteorological satellite was a groundbreaking development in atmospheric observation techniques. Meteorological satellites can obtain

*Corresponding author: SUN Jianhua, sjh@mail.iap.ac.cn

observations and distributions of data at higher spatial resolutions from larger coverage areas, thus alleviating greatly the problem of the lack of conventional data over oceanic, plateau, and desert areas. In particular, the Advanced TIROS-N Operational Vertical Sounder (ATOVS), on board the National Oceanic and Atmospheric Administration (NOAA) series of polar-orbiting satellites, has been providing atmospheric temperature and water vapor information, which are extremely important data for numerical weather prediction (NWP) (Andersson et al., 1994; Rabier et al., 2000). ATOVS radiance assimilation has improved forecasting significantly, not only in the southern hemisphere, but also in the northern hemisphere (Simmons and Hollingsworth, 2002). Better predictions of typhoon track were obtained through use of ATOVS radiances in global data assimilation at the Japan Meteorological Administration (Kazumori et al., 2003). Based on the three-dimensional variational (3DVAR) assimilation technique, direct assimilation of ATOVS microwave radiances were used to successfully simulate the fast movement of Typhoon Rammasun (2002) (Zhang et al., 2004), a feat unachievable with conventional radiosonde data.

However, radiance observations from satellites have biases which come from instrument characteristics, aging, pre-processing, and so on. Fast radiative transfer models also have biases from the approximation used to speed up the model and from the inaccuracy of spectroscopic databases. The biases of observations may distort the observed minus calculated (O–B) radiances and, sometimes, cause serious problems in the analyses (Okamato et al., 2005). Hence, bias in observed radiances, as well as those simulated from the model first-guess must be corrected. The original radiance-bias correction scheme used by the European Centre for Medium-Range Weather Forecasts (ECMWF) relied on the observed brightness temperatures from MSU (microwave sounder unit) channels as linear predictors. Many previous studies have proposed that bias in the O–B relies on the nature of air mass dependency (Kelly and Flobert, 1988; McMillin et al., 1989; Uddstrom, 1991; McNally et al., 2000). Minor improvements have been made by the use of cloudy radiances (Eyre, 1992), but the basic scheme has not been changed. Harris and Kelly (2001) took latitude-dependent scan correction into account and used the information from the model first-guess instead of MSU radiances as predictors. Liu et al. (2007) corrected the bias based on the scheme of Harris and Kelly (2001) and by taking into account both ATOVS instrument characteristics and weather conditions in China. Okamato et al. (2005) relied upon both the model first-guess and observed brightness temperatures from several AMSU-A (Advanced Microwave Sounding Unit A) channels (5, 7, and 10) as air mass bias predictors. The bias correction scheme used in this study was proposed by Harris and Kelly (2001, HK scheme), in which two kinds of observational biases are corrected, one dependent on the scan angles and the other on the categories of air mass.

In order to study the impact of ATOVS observations without and with bias correction, they were assimilated with an Ensemble Kalman Filter (EnKF) system based on the T106L19 forecast model. EnKF has emerged rapidly as the method of choice in the atmospheric and oceanographic sciences, as well as in satellite data assimilation, since it was first proposed by Evensen (1994). Satellite data has been assimilated by the EnKF system and the results indicate clear positive impacts (Miyoshi and Yoshiaki, 2007). Satellite wind data assimilated with the EnKF system have recently been applied to hurricane initialization (Chen and Snyder, 2006). There are several variants to the EnKF, a system first proposed by Evensen (1994), and then later by Houtekamer and Mitchell (1998). These variants include the use of the ensemble square root filter (EnSRF) (Whitaker and Hamill, 2002; Snyder and Zhang, 2003; Evensen, 2004; Zhang et al., 2006), the ensemble adjustment filter (EAF) (Anderson, 2001), and the ensemble transform Kalman filter (ETKF) (Bishop et al., 2001). In this paper, the EnSRF implemented by Whitaker and Hamill (2002) was used.

In this study, ATOVS observations with and without bias correction were assimilated with the EnSRF system, and then the results of the assimilation were used as the initial field of the T106L19 model to simulate the Typhoon Prapiroon (2006). In the following section, we describe the numerical prediction model and the fast radiative transfer model. In section 3, an independent bias correction scheme is employed to correct the observational bias. The method used for assimilating AMSU radiance data and the results of the numerical experiments are described in sections 4 and 5, respectively. Finally, conclusions and a discussion are presented in section 6.

2. Description of the models

2.1 *The numerical prediction model–**T***106***L***19

The global medium-range spectral model, T106L19, developed by the ECMWF was used for the numerical simulation of the typhoon. The "T" in the model's name refers to triangular truncation at 106 wave numbers, and the "L" to the fact that the model has 19 vertical layers with staggered variables. Using spherical harmonics as basic functions, the spectral form of the momentum, mass continuity, thermodynamics, mois-

ture conservation, and pressure tendency equations are expressed in terms of their coefficients. A semi-implicit time differencing scheme is used to enhance the time step for the gravitational modes. The vertical coordinate is based on a terrain-following σ-surface. For T106L19 representation, the Gaussian grid required is 320 by 160 points, corresponding approximately to a 1.125° grid. The time step is 900 seconds.

2.2 *The fast radiative transfer model–RTTOV-7*

RTTOV (Radiative Transfer for TIROS-N Operational Vertical Sounder) is a fast radiative transfer model which has been under development at the ECMWF since 1990 (Saunders et al., 1999). In this study, the fast radiative transfer model RTTOV-7 was used as the observation operator, $\boldsymbol{H}$, which is a nonlinear operator. The model allows rapid simulations of radiances for satellite infrared or microwave nadir scanning radiometers given an atmospheric profile of temperature, variable gas concentrations, and cloud and surface properties, referred to as the state vector (Saunders, 2005).

3. Radiance-bias correction and quality control

NOAA-16 is the fifth generation polar-orbiting routine environmental series satellite. The Advanced Microwave Sounding Unit (AMSU) onboard NOAA-16, which is used to improve the vertical sounding of atmospheric temperature and humidity, consists of type A (AMSU-A) with 15 channels (Table 1) and type B (AMSU-B) with 5 channels (Table 2). Compared to conventional infrared and visible light sounding units, the AMSU units have the unique ability to penetrate heavy clouds to sound the vertical structure of atmospheric temperature and humidity. The horizontal resolutions of AMSU-A and AMSU-B are 45 km and 15 km, respectively.

Table 1. AMSU-A channel characteristics.

Channel	Peak level	Main observation
1	surface	surface condition and the precipitable water
2	surface	surface condition and the precipitable water
3	surface	surface emissivity
4	1000 hPa	atmospheric temperature
5	700 hPa	atmospheric temperature
6	400 hPa	atmospheric temperature
7	270 hPa	atmospheric temperature
8	180 hPa	atmospheric temperature
9	90 hPa	atmospheric temperature
10	50 hPa	atmospheric temperature
11	25 hPa	atmospheric temperature
12	12 hPa	atmospheric temperature
13	5 hPa	atmospheric temperature
14	2 hPa	atmospheric temperature
15	surface	surface condition and the precipitable water

Table 2. AMSU-B channel characteristics.

Channel	Peak level	Main observation
1	surface	the precipitable water
2	surface	the precipitable water
3	440 hPa	atmospheric humidity
4	600 hPa	atmospheric humidity
5	800 hPa	atmospheric humidity

The correction scheme is divided into two steps. The first step is to use information on the scan angle to make a correction for the relative biases between measurements at different scan angles. The second step is to then correct the biases correlated with "air mass" as sensed by the measurements themselves. A brief description of the HK scheme follows below.

3.1 *Bias correction*

The scan correction has been subdivided into 18 latitude bands, each 10° in width. The scan correction is obtained using the formula:

$$d_{\rm s}(\phi,\theta) = \overline{D}_{\rm s}(\phi,\theta) - \overline{D}_{\rm s}(\phi,\theta=0)\,, \qquad (1)$$

where ϕ is the latitude band number, θ the scan angle, s the scan position, $\overline{D}$ the average observed radiance, and d the scan bias.

3.2 *Air mass bias correction*

The air mass regression scheme uses a set of bias predictors, $X_i (i = 1, \cdots, n)$, extracted from the same background state used in the EnKF system, to predict the radiance bias, B_j in each channel, j, through the linear regression equation

$$B_j = \sum_{i=1}^{n} A_{ji} X_i + C_j\,, \qquad (2)$$

where the coefficients A_{ji} and C_j are calculated by linear regression fit on a large sample, usually around two weeks of data. The coefficients are given by:

$$A_{ji} = \sum_{k=1}^{n} \langle D_j, X_k \rangle \cdot [\langle \boldsymbol{X}, \boldsymbol{X} \rangle]_i^{-1}\,, \qquad (3)$$

where $\langle \cdot\,, \cdot \rangle$ denotes covariance, $\boldsymbol{X}$ is the vector of X_i, D_j denotes the observation innovation in channel j, and k is the number of the predictors.

3.3 *Bias correction results*

According to the Eq. (2), air mass bias predictors should be set. There are high correlations between radiance bias, the thickness of 1000–300 hPa, 200–50 hPa, the surface skin temperature, and total precipitable water in the model first-guess (Harris and Kelly, 2001). Four predictors are the thicknesses (1000–300 and 200–50 hPa), the surface skin temperature, and the total precipitable water of the 6-h forecast with the T106L19 model. The analysis of the T106L19 model is derived from the EnSRF system.

As is well known, the period of corrected radiance data must be close to the period of radiance data that are used to calculate bias coefficients for the reason that the main changes in the air mass coefficients are related to seasonal changes and possible instrument drift. A large dataset, including AMSU-A and AMSU-B data and the 6-h forecast with the T106L19 model from 16–31 July 2006, were utilized to calculate coefficients of scan bias and air mass bias. Then, these coefficients were employed to correct radiance data after 31 July 2006.

Taking AMSU-A satellite radiance data from 1–15 August 2006 as an example to demonstrate the effect of bias correction, Fig. 1 shows mean O–B with and without bias correction. As can be seen, the mean O–B of the channels has been significantly reduced, and in more than half of the channels it successfully approaches zero after bias correction. However, the mean O–B in channels 1–3 and 13–15 is still high, with three possible reasons for this evident to the authors. Firstly, even if the bias correction scheme is perfect, O–B including a first-guess bias should be shifted from 0 by the effects of the first-guess bias. Secondly, channels 1–3 and 15 are highly sensitive to surface conditions, where the microwave surface emissivity is difficult to estimate accurately. And thirdly, the first-guess bias in the upper stratosphere may produce less accurate correction coefficients and predictors for channels 13 and 14. The peak O–B for each channel is shifted towards zero after bias correction (Fig. 2). The distribution of O–B after bias correction is more similar to a Gaussian distribution than without bias correction.

3.4 *Quality control*

Quality control is vital for any type of data. Many factors can cause large errors in satellite observations, such as weather conditions (clear, cloudy, or overcast), ground conditions (sea surface, land, sea ice etc.), geographical location (as in the mid latitudes or the tropics), observational locations (sub-satellite point or an edge measure), the response characteristics and accuracy in the process of the sensor moving in orbit, the error of the forward model and the error of the background field, and so on. In order to guarantee consistency between neighboring data and thus quality in analysis of results, quality control procedures must first be carried out. This was conducted in two steps, with the aim being to identify and reject bad radiance data. These two steps were: (1) radiance brightness temperature data outside of the interval 150–350 K were rejected; and (2) a check for departures between the simulated observation and the actual observation was carried out. Any radiance brightness temperature data that could not satisfy the following:

$$|\boldsymbol{u}_{i\_} - (\boldsymbol{H}\boldsymbol{x}_f)_i| < m\sigma_o \tag{4}$$

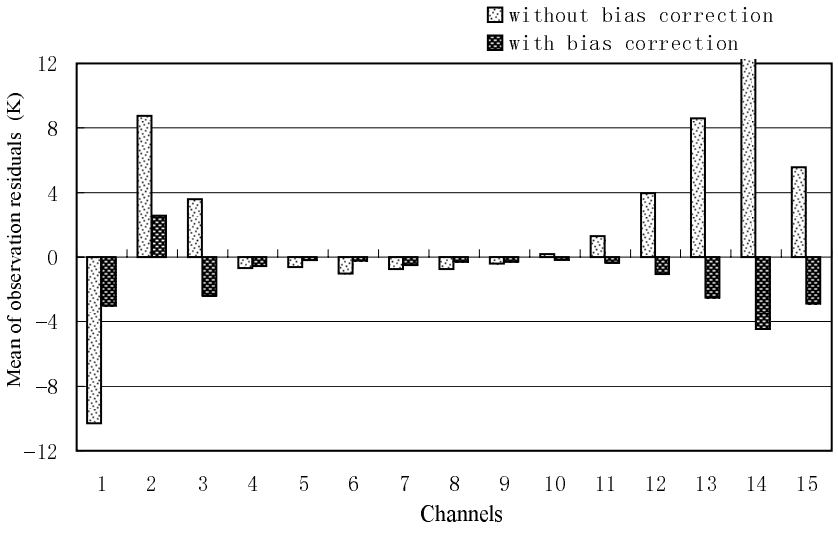

Fig. 1. Mean O–B (with and without bias correction) for AMAU-A channels 1–15 from NOAA16 radiance for the period 1–15 August 2006.

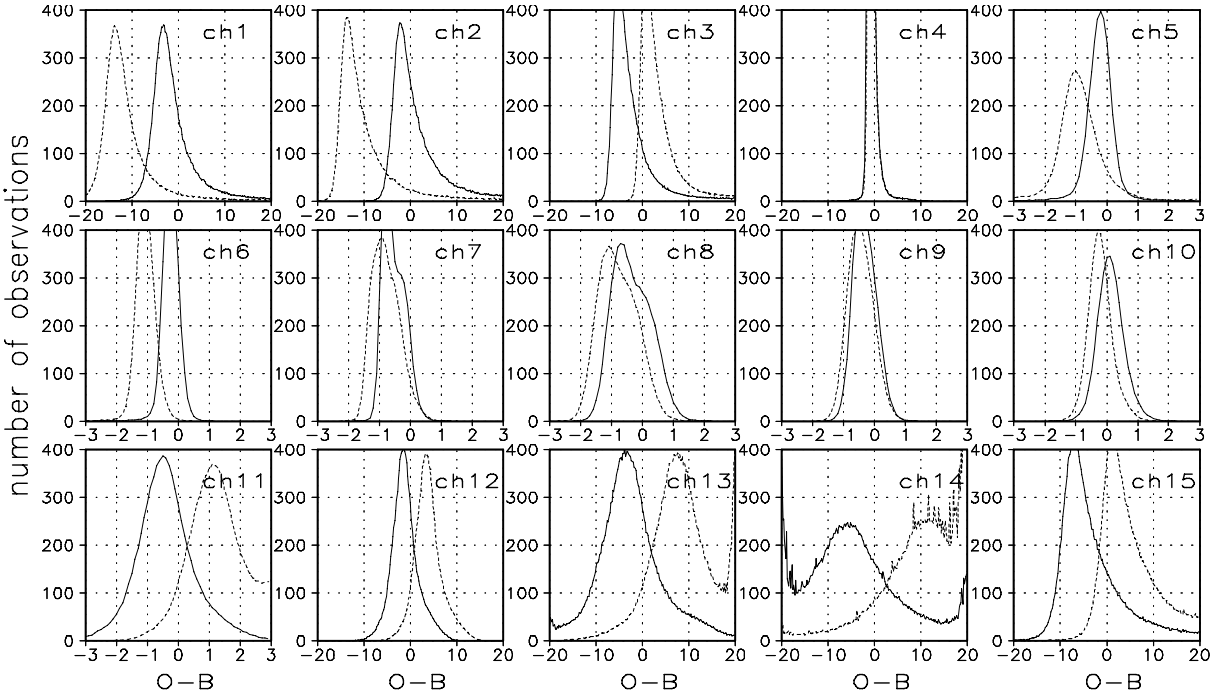

Fig. 2. Distribution of O–B for AMSU-A channels 1–15 for the period 1–15 August 2006. Heavy solid line, with bias correction; dotted line, without bias correction.

were excluded, where $\boldsymbol{y}_{j,\mathrm{o}}$ are the values of the actual observation in channel j, respectively; σ_o is the standard deviation of O–B; and m is a chosen parameter (m=3, in this experiment).

The selection of certain channels is determined by the conditions of each channel. Some channels were removed before undergoing subsequent quality control procedures. For instance, channels which are strongly sensitive to surface conditions (AMSU-A channels 1–3 and 15 and AMSU-B channels 1 and 2) were excluded because it is difficult to estimate the microwave surface emissivity accurately. As the mean of O–B was still large after bias correction (Fig. 1), channels 12–14 of the microwave sounder AMSU-A were also excluded, as well as in order to avoid the error caused by interpolating on the top level of the model, which might have influenced the retrieval results of temperature and water vapor.

4. The assimilation analysis algorithm for the ATOVS radiance data

4.1 *The EnSRF assimilation method*

Sampling error exists inevitably since the ensemble sizes are finite. In the ensemble-based Kalman filters, the sampling error reduces the accuracy of the analysis-error covariance. To eliminate the sampling error associated with the perturbed observations and to embody the observation-error covariance in the analysis-error covariance, some schemes without perturbed observations are proposed, in which EnSRF is a simple and feasible one.

In the Kalman Filter, the minimum error-variance estimate of the analyzed state x_a is given by

$$\boldsymbol{x}_\mathrm{a} = \boldsymbol{x}_\mathrm{f} + \boldsymbol{K}(\boldsymbol{y}_\mathrm{o} - \boldsymbol{H}\boldsymbol{x}_\mathrm{f}) \,, \tag{5}$$

where $\boldsymbol{x}_\mathrm{f}$ is the model forecast, $\boldsymbol{y}_\mathrm{o}$ is a set of observations, $\boldsymbol{H}$ is an observation operator that converts the model state to the observation space, and $\boldsymbol{K}$ is Kalman gain matrix. Expressing the variables as an ensemble mean (denoted by an overbar) and a deviation from the mean (denoted by a prime), updated equations for the EnKF system can be written as

$$\overline{\boldsymbol{x}}_\mathrm{a} = \overline{\boldsymbol{x}}_\mathrm{f} + \boldsymbol{K}(\overline{\boldsymbol{y}}_\mathrm{o} - \boldsymbol{H}\overline{\boldsymbol{x}}_\mathrm{f}) \,, \tag{6}$$

$$\boldsymbol{x}'_\mathrm{a} = \boldsymbol{x}'_\mathrm{f} + \widetilde{\boldsymbol{K}}(\boldsymbol{y}'_\mathrm{o} - \boldsymbol{H}\boldsymbol{x}'_\mathrm{f}) \,, \tag{7}$$

where $\boldsymbol{K}$ is the Kalman gain and $\widetilde{\boldsymbol{K}}$ is the gain used to update deviations from the ensemble mean. The EnSRF algorithm eliminates the necessity to perturb the observations, and Eq. (6) is simplified to:

$$\boldsymbol{x}'_\mathrm{a} = \boldsymbol{x}'_\mathrm{f} + \widetilde{\boldsymbol{K}}\boldsymbol{H}\boldsymbol{x}'_\mathrm{f} \,. \tag{8}$$

$\widetilde{\boldsymbol{K}}$ is defined by Whitaker and Hamill (2002) as:

$$\widetilde{\boldsymbol{K}} = \left(1 + \sqrt{\frac{\boldsymbol{P}_f}{\boldsymbol{H}\boldsymbol{P}_f\boldsymbol{H}^{\mathrm{T}} + \boldsymbol{R}}}\right)^{-1} \boldsymbol{K} \,. \qquad (9)$$

This definition for $\widetilde{\boldsymbol{K}}$ is the analysis-error covariance of an ensemble remaining the same as in the EnKF system. Here, $\boldsymbol{H}\boldsymbol{P}_{\mathrm{f}}\boldsymbol{H}^{\mathbf{T}}$ and $\boldsymbol{R}$ are scalars representing the background and observational-error variance at the observation location.

4.2 *The initial ensemble perturbations*

The original data assimilation system of T106L19 is Optimal Interpolation (OI). The EnSRF data assimilation system based on the global medium-range spectral model T106L19 has been newly developed by our group, in which the initial ensemble perturbations are based on the multivariate empirical orthogonal function (MEOF). The initial ensemble mean state is taken from the OI analysis and there are five variables in the state vector: $\boldsymbol{U}$ (zonal wind), $\boldsymbol{V}$ (meridional wind), $\boldsymbol{T}$ (temperature), $\boldsymbol{q}$ (specific humidity), and $\boldsymbol{p}$ (surface pressure).

5. Numerical experiments

5.1 *A brief description of Typhoon Prapiroon*

Typhoon Prapiroon (2006) formed in the middle of the South China Sea near (17.0°N, 117.8°E) on 1 August 2006. Moving northwestward, it reached the intensity of a typhoon after one day. It then moved west-northwestwards to the western coast of Guangdong and landed during the night of 3 August, with a maximum wind speed of 33 m s^{-1} during landfall. Thereafter, it weakened to a tropical storm as it moved on to Guangxi Province on 4 August. Typhoon Prapiroon (2006) brought heavy rainfall in many provinces following landfall, although its lifetime was only four days. In the experiment, the simulation period was taken as 1800 UTC 2 August 2006 to 1200 UTC 4 August 2006, with the aim to investigate the impact of radiance-bias correction on the prediction of Prapiroon's track.

5.2 *Experimental setup*

To investigate the impact of ATOVS microwave radiance-bias correction on the prediction of typhoon track, two experiments were carried out. In the first experiment (Expt. 1), radiosonde data and ATOVS microwave radiance brightness temperatures without bias correction were adopted as the observation data. The analysis period was from 0000 UTC 1 August to 1200 UTC 2 August, and observations were taken every 6 h. The final analysis was used as the initial fields of the T106L19 model for the 48-h simulation. The predictions were outputted every 6 h from 1800 UTC 2 to 1200 UTC 4 August 2006. In the second experiment (Expt. 2), ATOVS microwave radiance brightness temperatures with bias correction were adopted as observation data, instead of without, as in Expt. 1. All other factors were the same as in Expt. 1.

The resolution for ATOVS observations was selected as 250 km for AMSU-A, and 180 km for AMSU-B. The coverage of the ATOVS observations, obtained every 6 h, is shown in Fig. 3. The covariance localization based on Gaspari and Cohn (1999) was used for the two experiments. The ensemble size was fixed at 80, and the covariance localization radius was fixed at 1000 km.

5.3 *Analysis of results*

Figure 4 shows the initial location (1200 UTC 2

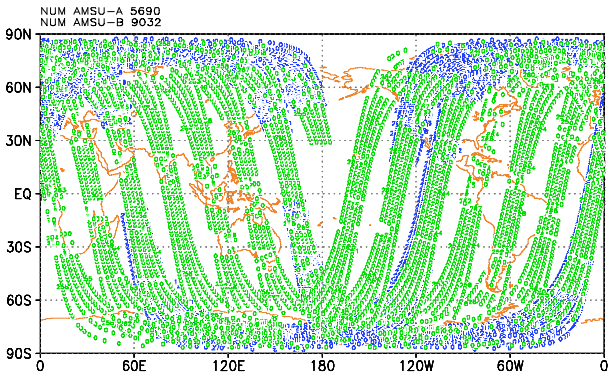

Fig. 3. Observational coverage of ATOVS data every six hours. Green, AMSU-A; blue, AMSU-B.

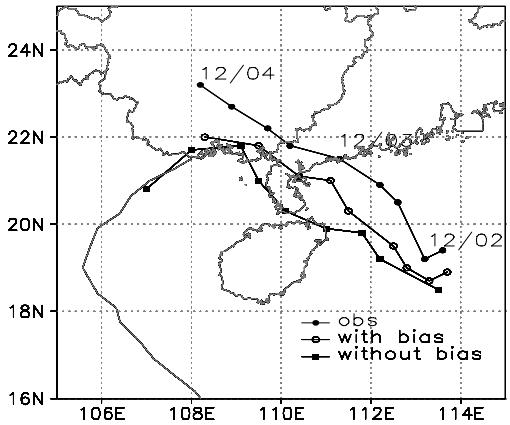

Fig. 4. Initial location (1200 UTC 2 August) and the predicted tracks of the typhoon from 1800 UTC 2 August to 1200 UTC 4 August 2006 at 6-h intervals. Solid dotted line, observed typhoon position; hollow dots, position of Expt. 2; squares, Expt. 1.

August), the predicted track, and the observed best track (OBS) from 1800 UTC 2 August to 1200 UTC 4 August 2006. Both the moving direction and the speed of the typhoon from Expt. 1 and Expt. 2 are similar to those of the OBS, except for the 48-h prediction in Expt. 1. However, a better result was obtained in Expt. 2, in spite of the fact that the simulated location of the typhoon moves towards the south in comparison with the OBS.

Expt. 2 shows the typhoon to be moving southwestward from 1200 UTC to 1800 UTC 2 August, which is similar to the track of the OBS. The position of landfall in Expt. 1 is far from the observation. At first, the typhoon in Expt. 1 lands on the northeast of Hainan Province, with its center located at (19.9°N, 111.0°E) at 0600 UTC 3 August, and then it lands secondly on the western coast of Guangdong at 1200 UTC 3 August, while the observed position of the typhoon's landfall was at about (21.4°N, 111.6°E) in Guangdong Province at 1200 UTC 3 August. In Expt. 2, the typhoon landing on the southwest coast of Guandong Province, which is near to the observed position, despite a time lag of about 9 h compared to the observation. Furthermore, the track error in Expt. 1 increased to more than 260 km for the 48-h prediction, while the error in Expt. 2 was about 150 km for the same period.

Let us now turn our attention to the circulation at 500 hPa and its impacts on Typhoon Prapiroon (2006). NCEP reanalysis data are used to verify the simulations. Geopotential height in the NCEP reanalysis at 500 hPa at 1200 UTC 2 August shows that the center of the West Pacific Subtropical High (WPSH) is located at the Sea of Japan, with its western point at around 119°E (Fig. 5a1). Subsequently, the WPSH intensifies gradually and extends westward. At 1200 UTC 3 August, the intensity of the WPSH reaches 5940 gpm, with its western point extending

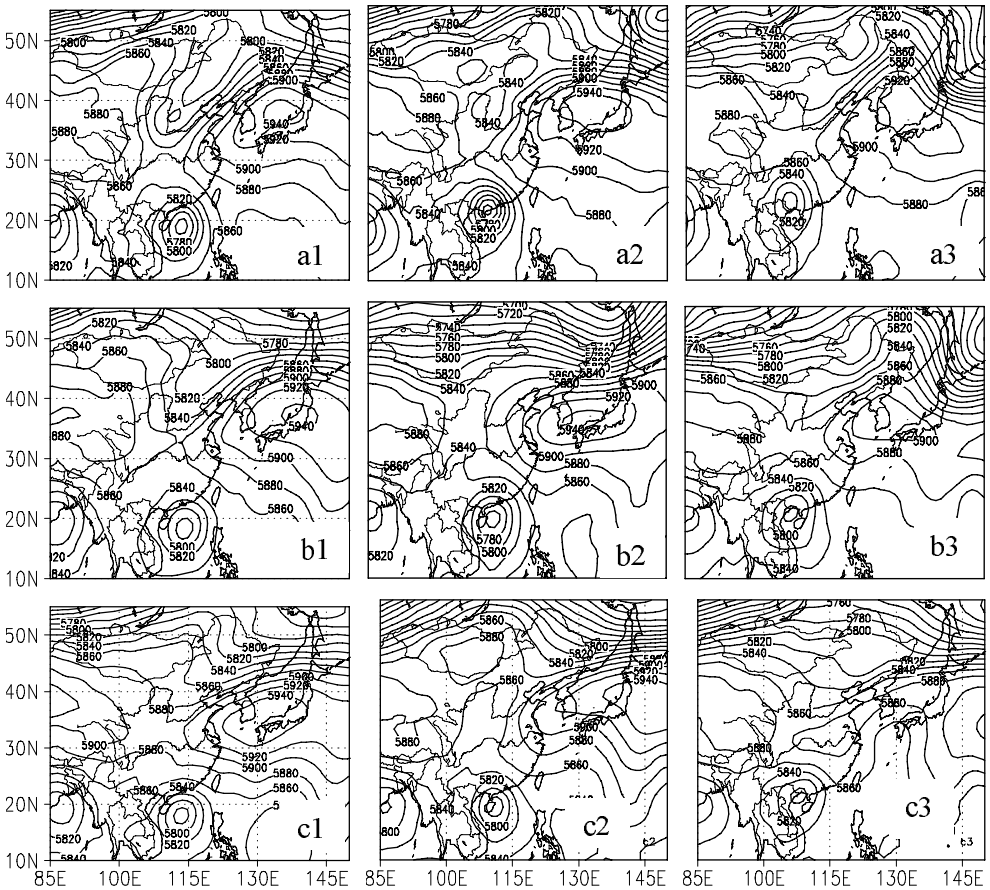

Fig. 5. Geopotential height at 500 hPa on 1200 UTC 2 August (a1, b1, c1), 1200 UTC 3 August (a2, b2, c2) and 1200 UTC 4 August 2006 (a3, b3, c3). The upper panel (a1, a2, a3) is the NCEP reanalysis; (b1) is the initial circulation with bias correction of Expt. 2; (c1) is the initial circulation without bias correction of Expt. 1; (b2) and (b3) are the predictions with bias correction; and (c2) and (c3) are the predictions without bias correction. (Units: gpm)

to around 114°E (Fig. 5a2). At the same time, high pressure over northeastern China strengthens gradually and moves eastward. At 1200 UTC 4 August, high pressure over northeastern China, which arises northward of the WPSH (Fig. 5a3), moves eastward to the coastal area of northeastern Asia. Under such an influence of the WPSH, Typhoon Prapiroon (2006) moves westward after landfall.

The initial circulations (the final analysis fields) are shown in Figs. 5b1 and 5c1 to show the influence of bias correction. In the middle and high latitudes, two high pressure patterns and one low pressure pattern can be found in Expt. 1 and Expt. 2, but the circulation in Expt. 2 is more consistent with NCEP reanalysis data (Fig. 5a1). In Expt. 1, the center of the WPSH is located further west. The more southward the location of the WPSH, the more southward the track of the typhoon. There is a significant difference from NCEP reanalysis data in Expt. 1. The high pressure ridge over northwestern China is obviously stronger and the center of the WPSH further east (Figs. 5c2 and 5c3). After 0600 UTC 4 August, the intensity of the WPSH is stronger over the middle and lower reaches of the Yangtze River, which induces southwestward movement of Typhoon Prapiroon (2006), so that the prediction error of the typhoon track becomes larger in Expt. 1. The intensity of the typhoon at 500 hPa (about 5760 gpm) in Expt. 2 is better than in Expt. 1 (about 5780 gpm) from 1800 UTC 2 to 1800 UTC 3 August, although it is still weaker than that of the NCEP reanalysis (about 5740 gpm). The results of the simulation using ATOVS radiance with bias correction (Expt. 2) show that the position, intensity and movement of the WPSH are more consistent with the NCEP reanalysis (Figs. 5b2 and 5b3), such that the prediction of typhoon track is more similar to the OBS. Based on the above analyses, it can be concluded that the predicted circulation in Expt. 2 is better than in Expt. 1.

6. Conclusions and discussion

In this paper, the HK scheme was adopted to correct the bias between observed Advanced TIROS-N Operational Vertical Sounder (ATOVS) radiances and those simulated from the T106L19 model first-guess. The corrected ATOVS data were then used to simulate Typhoon Prapiroon (2006), which occurred during the period 2–4 August 2006. The EnKF system based on the T016L19 model was used to directly assimilate ATOVS microwave radiance observations with and without bias correction, and the final analysis was used as the initial conditions of the T106L19 model to simulate Typhoon Prapiroon (2006). The impact of radiance-bias correction was then analyzed. The following can be concluded:

(1) The mean values of O–B in most channels come closer to zero, and the peak in each channel shifts towards zero, after bias correction. Furthermore, the distribution of O–B is more similar to a Gaussian distribution than without bias correction.

(2) The assimilation of ATOVS radiance data with bias correction has a positive impact on the prediction of typhoon track and intensity.

(3) With the rapid development of assimilation and remote sensing sounding techniques, unconventional satellite observations are increasingly used to improve numerical prediction. The results of the experiments in the present study and previous studies show that the technique of removing bias in radiance is an effective way to better use satellite data. Thus, it has great potential and brilliant prospects in the prediction of typhoon tracks.

This study is only a case study at present. In the future, more experiments with other real cases, along with further studies of bias correction, including sensitivity studies on the impact of different O–B datasets for specifying bias correction coefficients, will bring more insights into this problem.

Acknowledgements. The authors express their sincere thanks to the Editor and two anonymous reviewers for their constructive comments and suggestions, which helped to improve the representation of the paper. This research was supported by the Knowledge Innovation Program of the Chinese Academy of Sciences (Grant Nos. KZCX2-YW-202 and KZCX2–YW–Q03–3) and the Chinese Special Scientific Research Project for Public Interest (Grant No. GYHY200906004). The authors would like to express their great appreciation to Dr. ZHENG Fei and Dr. GUO Zhenghai of the Institute of Atmospheric Physics for their help.

REFERENCES

Andersson, E., J., Pailleux, J. N. Thepaut, J. R. Eyre, A. P. McNally, G. A. Kelly, and P. Courtier, 1994: Use of cloud-cleared radiances in three/four-dimensional variational data assimilation. *Quart. J. Roy. Meteor. Soc.*, **120**, 627–653.

Anderson, J. L., 2001: An ensemble adjustment Kalman filter for data assimilation. *Mon. Wea. Rev.*, **129**, 2284–2903.

Bishop, C. H., B. J. Etherton, and S. J. Majumdar, 2001: Adaptive sampling with the ensemble transform Kalman filter. Part I: Theoretical aspects. *Mon. Wea. Rev.*, **129**, 420–436.

Chen, L. S., 1997: The prediction of typhoons with asymmetrical structure and sudden change in movement. *Guangdong Meteorology*, Suppl. 3, 12–13. (in Chi-

nese)

Chen, L. S., and Z. Meng, 2001: An overview on tropical cyclone research progress in China during the past ten years. *Chinese J. Atmos. Sci.*, **25**(2), 420–432. (in Chinese)

Chen, Y., and C. Snyder, 2006: Initializing a Hurricane Vortex with an Ensemble Kalman Filter. *27th Conference on Hurricanes and Tropical Meteorology,* American Meteorological Society, Monterey, CA. Paper 8A.5.

Ding, Y. H., 1991: *Advanced Synoptic Meteorology.* China Meteorological Press Beijing, 792pp. (in Chinese)

Evensen, G., 1994: Sequential data assimilation with a nonlinear quasi-geostrophic model using Monte Carlo methods to forecast error statistics. *J. Geophys. Res.*, **99**, 10143–10162.

Evensen, G., 2004: Sampling strategies and square root analysis schemes for the EnKF. *Ocean Dynamics*, **54**, 539–560.

Eyre, J. R., 1992: A bias correction scheme for simulated TOVS brightness temperatures. *Technical Memorandum*, **176**, 81–109.

Gaspari, G., and S. Cohn, 1999: Construction of correlation functions in two and three dimensions. *Quart. J. Roy. Meteor. Soc.*, **125**, 723–757.

Harris, B. A., and G. Kelly, 2001: A satellite radiance bias correction scheme for data assimilation. *Quart. J. Roy. Meteor. Soc.,* **127**, 1453–1468.

Houtekamer, P. L., and H. L. Mitchell, 1998: Data assimilation using an ensemble Kalman filter technique. *Mon. Wea. Rev.*, **126**, 796–811.

Kazumori, M., K. Okamoto, and H. Owada, 2003: Operational use of the ATOVS radiances in global data assimilation at the JMA. *Proc. Thirteenth International TOVS Study Conference*, Sainte-Adéle, Québec, Canada, 29 October–4 November 2003, 37–42.

Kelly, G., A., and J. F. Flobert, 1988: Radiance tuning. *Tech. Proc. 4th Int. TOVS Study Conference*, Igls, Austria, Cooperative Institute for Meteorological Satellite Studies, Space Science and Engineering Center, University of Wisconsin, USA.

Liu, Z. Q., F. Y. Zhang, X. B. Wu, and J. Xue, 2007: A regional ATOVS radiance-bias correction scheme for radiance assimilation. *Acta Meteorologica Sinica*, **65**(1), 113–123. (in Chinese)

McMillin, L. M., L. J. Crone, and D. S. Crosby, 1989: Adjusting satellite radiances by regression with an orthogonal transformation to a prior estimate. *J. Appl. Meteor.*, **28**, 969–975.

McNally, A. P., J. C. Derber, W. Wu, and B. B. Katz, 2000: The use of TOVS level-1b radiances in the NCEP SSI analysis system. *Quart. J. Roy. Meteor. Soc.*, **126**, 689–724.

Meng, Z., L. S. Chen, and X. D. Xu, 2002: Recent progress on tropical cyclone research in China. *Adv. Atmos. Sci.*, **19**(1), 103–110.

Miyoshi, T., and S. Yoshiaki, 2007: Assimilating satellite radiances with a Local Ensemble Transform Kalman Filter (LETKF) applied to the JMA Global Model (GSM). *SOLA*, **3**, 037–040.

Okamoto, K., M. Kazumori, and H. Owada, 2005: The assimilation of ATOVS radiances in the JMA global analysis system. *J. Meteor. Soc. Japan*, **83**(2), 201–217.

Rabier, F., J. Jarvinen, E. Klinker, J. F. Mahfouf, and A. Simmons, 2000: The ECMWF implementation of four-dimensional variational assimilation. I: Experimental results with simplified physics. *Quart. J. Roy. Meteor. Soc.*, **126**, 1143–1170.

Saunders, R., 2005: RTTOV-7 users guide. ECMWF Technical Memo., No. 345**.**

Saunders, R. W., M. Matricardi, and P. Brunel, 1999: An improved fast radiative transfer model for assimilation of satellite radiance observations. *Quart. J. Roy. Meteor. Soc.*, **125**, 1407–1425.

Simmon, A., and A. Hollingsworth, 2002: Some aspects of the improvement in skill of numerical weather prediction. *Quart. J. Roy. Meteor. Soc.*, **128**, 647–687.

Snyder, C., and F. Zhang, 2003: Assimilation of simulated Doppler radar observations with an ensemble Kalman filter. *Mon. Wea. Rev.*, **131**, 1663–1677.

Uddstrom, M., 1991: Forward model errors. *Proc. 6^{th} Int. TOVS Study Conference,* Airlie, Virginia, Cooperative Institute for Meteorological Satellite Studies, Space Science and Engineering Center, University of Wisconsin, USA, 501–516.

Whitaker, J. S., and T. M. Hamill, 2002: Ensemble data assimilation without perturbed observations. *Mon. Wea. Rev.*, **130**, 1923.

Zhang, F., Z. Meng, and A. Aksoy, 2006: Test of an ensemble-Kalman filter for mesoscale and regional scale data assimilation. Part I: Perfect-model experiments. *Mon. Wea. Rev.*, **134**, 722–736.

Zhang, H., J. Xue, G. Zhu, S. Y. Zhuang, X. B. Wu, and F. Y. Zhang, 2004: Application of direct assimilation of ATOVS microwave radiances to typhoon track prediction. *Adv. Atmos. Sci.*, **21**(2), 283–290.